periodica polytechnica

Electrical Engineering
53/3-4 (2009) 91–97
doi: 10.3311/pp.ee.2009-3-4.01
web: http://www.pp.bme.hu/ee

RESEARCH ARTICLE

3SC Control for high efficiency grid connected photovoltaic converters

Attila Balogh / *István* Varjasi

Received 2010-05-22

Abstract

Nowadays there are several grid connected converters in the grid system. These grid connected converters are generally the converters of renewable energy sources, industrial four quadrant drives and other converters with DC link. These converters are connected to the grid typically through a three phase IGBT bridge. The standards prescribe the permissible maximal harmonic emission and the maximal reactive current for the grid connected converters. For a converter working at nominal power these two prescriptions together mean almost unity power factor. The harmonic emission could be easily limited with high switching frequency and/or with large harmonic filters. Further financial viewpoints are the efficiency, the small size and weight. Comparing to traditional control these requirements can be simultaneously satisfied much better with the 3SC (three state control) method. At 3SC we utilize all the three allowed state of one arm of the IGBT bridge, i.e. upper part conducting, lower part conducting, none of them conducting.

Keywords

PV converter · three state control · discontinuous current · control method · high efficiency

Attila Balogh
Department of Automation and Applied Informatics, BME, H-1111, Budapest, Hungary
e-mail: balogh@aut.bme.hu

István Varjasi
Department of Automation and Applied Informatics, BME, H-1111, Budapest, Hungary
e-mail: varjasi@aut.bme.hu

1 Introduction

Nowadays in applications of renewable energy sources it is important to develop powerful and energy-saving photovoltaic converters and to keep the prescriptions of the standards. The improved efficiency of PV converters and the decreasing price of PV cells lead to the widespread utilization of this kind of renewable energy. During last decade some software and hardware solutions have been developed for increasing the efficiency depending on PV converter type. The inverter represents about 10-15% of the total investment cost of a grid connected system. Thanks to the development of PV inverter in small to medium power range the inverter cost of this power class has decreased by more than 50% during the last 10 years. The main causes for this reduction are the increase of the production quantities and the implementation of new system technologies [1]-[5]. The ratio of the cell/converter price has not been changed significantly. This also means that 1% improvement of the efficiency causes about 10% more valuable converter. The industrial PV converters consist of PV array, Boost DC/DC converter and the three phase inverter with filters (Fig. 1).

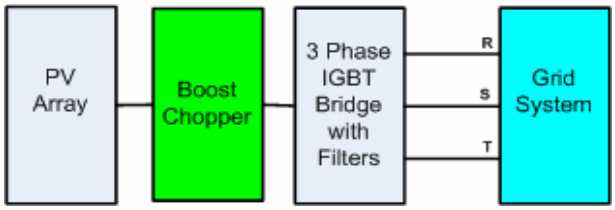

Fig. 1. Topology of the converter

The PV array converts the solar energy to DC power; the optional step-up converter may raise the voltage level of the PV array to the voltage level of the three phase bridge. The control of the boost chopper algorithm includes the maximal power point tracking (MPPT). The reference for the PV voltage comes from the MPPT and the actual PV voltage controlled by the booster current. The DC link voltage is controlled to be a few per cent above the peak line voltage. The DC voltage is controlled in a cascade structure where the inner loop controls the active component of the grid current. The high order harmonics

of the output current are filtered out by passive low-pass filters. The reactive part of the inverter current is controlled to compensate the reactive current component caused by the filter. In most cases there is a transformer between the converter and the grid. It is used for galvanic isolation and helps against the DC current injection into the grid. In the USA the transformer is mandatory while in the EU it is only optional. However, when a transformer is used we have some freedom for the common mode voltage of the converter. The most financial viewpoint of a PV converter is the efficiency. In case of grid connected PV converters the obvious solution to increase the efficiency is to reduce the switching losses. In order to increase the efficiency the developers make effort with designing sophisticated main circuit and implementing new control strategies. Adding new features to the main circuit is very expensive and time-consuming, so in the most cases gives unacceptable results. In contrast of this the implementation of new algorithms results the negligible increase of repetitive costs. In case of given power, voltage and current the efficiency can be affect from control side with the change of modulation techniques. When the DC link voltage is not significant higher ($<15\%$) than the peak line voltage of the grid, the switching losses can be efficiently decreased ($\approx 50\%$, [1]) with Flat-top modulation. The aforementioned voltage ratio exists when the PV voltage in MPP is less than the peak line voltage of the grid, namely booster is needed. As in [6]-[9] can be seen in case of single phase inverters on low power level good efficiency can be reached with the 3SC modulation. In this article such three phase control is presented which joins the benefits of the aforementioned two methods.

2 Standard control

During the last decade some control method has been developed for grid connected PV converters. Most of them consist of an outer DC voltage control loop involving the Maximal Power Point Tracking (MPPT) method and inner current control loop. From these traditional controls we use the grid voltage oriented current control. This control structure is very similar to the field oriented control (FOC) of AC machines. However, the traditional control is completed with auxiliary methods. The controllers work here also in a rotating frame, but this rotating frame is connected to the grid voltage vector, so this control system can be named as grid voltage oriented control (GVOC). The component of the current vector in the direction of the grid voltage vector is named as current "d" and is proportional to active power, while the orthogonal current component is named as current "q" and is proportional to reactive power. In this arrangement (see Fig. 2) there is no zero order current, so it is enough to measure only two currents. The phase currents are transformed to the rotating d-q coordinate-system [2]. For the current control the currents are sampled at symmetry point(s) of the PWM cycle (i.e. at the peaks of the up-down counter), so the sampled current is close to the average value for a given switching period.

3 The 3SC Control

At 3SC we utilize all the three allowed state of one arm of the IGBT bridge, i.e. upper part conducting, lower part conducting, none of them conducting. E.g. for a switching period where the reference for $i_a > 0$, 1H will be controlled according to the output of the current controller, where 1L will be disabled for the whole switching period. The newly developed inverter control has to satisfy two groups of requirements. On one hand the DC source energy should be feed-backed to the AC network with efficiency as high as possible. On the other hand the prescriptions of the harmonic emission standards must be fulfilled for the utility compatibility. According to the standards [UL1741], the AC currents should be nearly sinusoidal (the THD total harmonic distortion has to be less than 5%), and the power factor should be greater than 0.95.

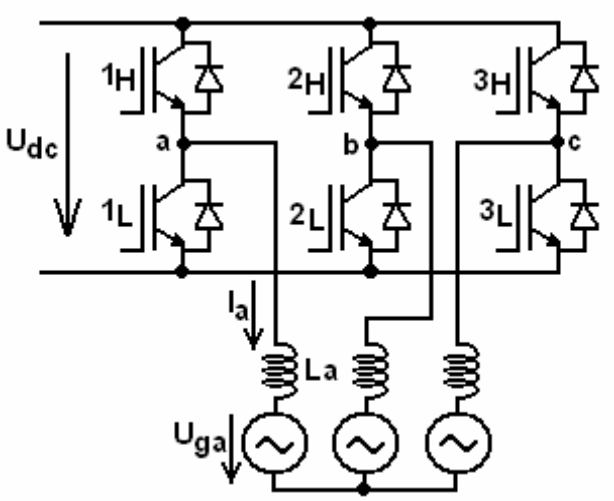

Fig. 2. The main circuit

By reduction of the switching losses with the proposed method we may increase the efficiency while maintaining the limitations of standards. There are some calculation modes of the PV converter's efficiency. From these we use the EU efficiency which can be calculated as the weighted averages of efficiencies measured at the 5%, 10%, 20%, 30%, 50% and 100% of nominal power according to the standard. With the traditional control it is very hard to reach a good efficiency below 10% of nominal load, since the iron losses of the filter choke will be the same and the switching-off losses of the IGBT-s will be comparable to the losses at nominal load. Our method increases the efficiency when the load is below 10%.

The new control algorithm reaches the better efficiency utilizing the 3SC method. With this control the switching-on losses of the IGBT would be zero, the iron losses and the switching-off losses would be smaller. While the idea seems quite simple, the method is very complicated, since the current of the three phases are not independent, and the discontinuous phase reacts on the voltage of the other phases. Unlike with traditional control, there is no symmetry point of the switching period, so the sampled current will not be equal to the average current. In the

following we will introduce a method how this relationship can be calculated in continuous and discontinuous current mode.

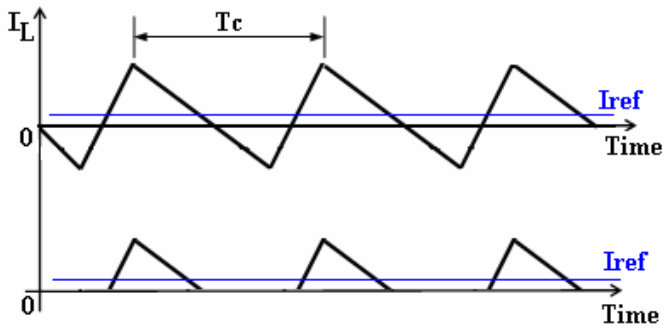

Fig. 3. Current waveforms

The current waveforms with traditional and 3SC method can be seen in Fig.3. Let us assume that the DC link voltage approximately equals to the peak line voltage of the grid and that moment is investigated when the AC voltage equals to the DC link voltage and the power factor is close to one. With these conditions the current ripple will be the largest in the phase where the current reference is the smallest. The upper curve is the continuous while the lower one is the 3SC waveform. With the traditional control IGBT 2H and 2L of the middle leg with near 50% duty cycle make the almost zero voltage of the phase b. The current of the phase b with a small average value fluctuates between positive and negative values (see upper curve at Fig.3). The cyclic change would result significant switching and iron losses. With the 3SC method only the upper IGBT of the middle leg (the IGBT in the direction of the reference current) will be switched (see lower curve at Fig. 3) causing discontinuous current mode. With 3SC the switching-on losses will be zero, since the current at switching-on is zero and due the smaller current ripple the iron and switching-off losses will be smaller assuming constant switching frequency.

In the first step in order to simplify the mathematical model we prescribed some simplifications and limitations. These are the followings:

- the converter should create only negligible reactive power,
- in the phase where the absolute value of the current reference is the highest, one IGBT is switched on for the whole switching period,
- at least in two inductors the currents are continuous for one switching period,
- the grid voltage is symmetrical.

These limitations are true for the most grid connected PV converters. The mathematical description of the model without any simplification is quite complicated, so due the available length of this article it is not investigated in it.

The 3SC method is investigated only in the first control section, in which the line voltage between a and c phases reaches its positive maximum. In this case IGBT 1H and 3L will have near 100% duty cycle (see Fig.2) and the following conditions are valid

- $U_a > U_b$; $U_b > U_c$ and $U_b < 0$.

Considering similar conditions there are 12 control sections. In this paper only the first control section's equations are obtained, the other 11 states can be calculated from these, with rotating the voltage vectors.

3.1 The continuous operational mode

The continuous current mode waveforms for a given switching period can be seen in Fig. 4. The upper part of the figure represents the states of the semiconductors. In continuous current mode there are three different switching states (see Fig. 4), in the first one 1H IGBT, the diode of 2H and 3H IGBT-s conduct the current, in the second one 1H IGBT, the diode of 2H IGBT and 3L IGBT, while in the third one 1H, 2L, 3L IGBTs are conducting the current.

In the first step the change of rate of inductor currents is calculated in the three switching states.

The change of rate of inductors current in the first switching state in phase b and c is the following:

$$\frac{di_{b1}}{dt} = -\frac{u_{gb}}{L}, \frac{di_{c1}}{dt} = -\frac{u_{gc}}{L}, \tag{1}$$

where u_{gb} and u_{gc} are the grid voltages and L is the grid side inductance of the converter.

In the second switching state the rates are:

$$\frac{di_{b2}}{dt} = \frac{-3u_{gb} + u_{dc}}{3L}, \frac{di_{c2}}{dt} = \frac{-3u_{gc} - 2u_{dc}}{3L}. \tag{2}$$

While in the third one:

$$\frac{di_{b3}}{dt} = \frac{-3u_{gb} - u_{dc}}{3L}, \frac{di_{c3}}{dt} = \frac{-3u_{gc} - u_{dc}}{3L}. \tag{3}$$

For repetitive current waveform in steady state t_{1f} and t_{2f} switching times can be approximated as:

$$t_{1f} = \frac{U_{ga} - U_{gb}}{U_{dc}} T_c, \tag{4}$$

$$t_{2f} = \frac{U_{ga} - U_{gc}}{U_{dc}} T_c, \tag{5}$$

where T_c is the PWM cycle time, U_{ga} is the average value of $u_{ga}(t)$ for the inspected switching period.

Since the PWM period does not have symmetrical points (see above) for the current control the relationship between the average value and the sampled value of the inductors currents has to be calculated.

The current in phase b at the end of switching states can be calculated from (1) (2) (3) and (4) (5) as follows:

$$i_{b1} = i_{b0} + \frac{di_{b1}}{dt}(T_c - t_{2f}). \tag{6}$$

$$i_{b2} = i_{b1} + \frac{di_{b2}}{dt}(t_{2f} - t_{1f}). \tag{7}$$

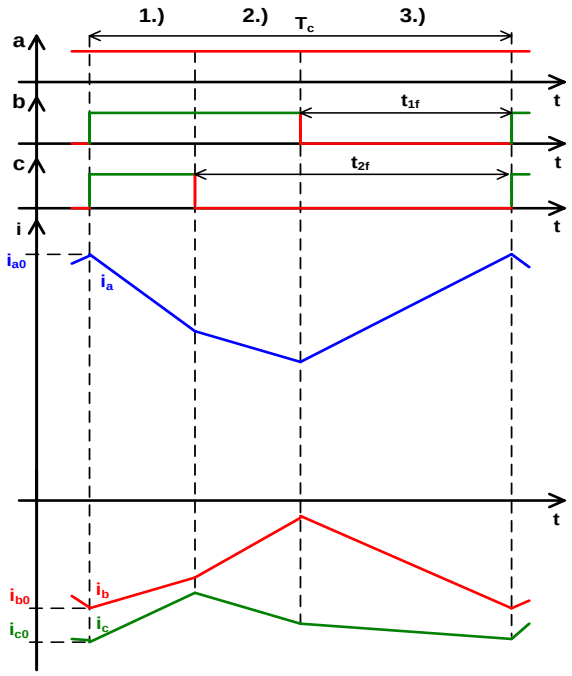

Fig. 4. Continuous waveforms

$$i_{b3} = i_{b2} + \frac{di_{b3}}{dt} t_{1f} \quad , \tag{8}$$

where i_{b1} is the phase b current at the end of the first switching state, i_{b2} is at the end of second switching state, while i_{b3} is at the end of the PWM cycle time.

In steady state the current at the start and at the end of the PWM cycle time should be equal ($i_{b3} \approx i_{b0}$), so the sum of the current changes is zero:

$$\frac{di_{b1}}{dt}(T_c - t_{2f}) + \frac{di_{b2}}{dt}(t_{2f} - t_{1f}) + \frac{di_{b3}}{dt} t_{1f} = 0. \tag{9}$$

From (6) (7) (8) and (9) the average value of the phase b current can be calculated as follows:

$$i_{bAV} = \frac{1}{T_c}\left(\frac{i_{b0} + i_{b1}}{2}(T_c - t_{2f}) + A\right), \quad \text{where}$$
$$A = \frac{i_{b1} + i_{b2}}{2}(t_{2f} - t_{1f}) + \frac{i_{b2} + i_{b3}}{2} t_{1f}. \tag{10}$$

Substituting (4) (5) in (10) the average value of the current in phase b is:

$$i_{bAV} = i_{b0} - \frac{T_c}{6LU_{dc}}\left[U_{gb}(3U_{dc} + 7U_{gb}) + U_{gc}(4U_{gb} - 2U_{gc})\right] . \tag{11}$$

The average value of phase c current can be calculated similarly to phase b. Without demonstration the average value of phase c is:

$$i_{cAV} = i_{c0} - \frac{T_c}{6LU_{dc}}\left[U_{gc}(3U_{dc} + 7U_{gc}) + U_{gb}(4U_{gc} - 2U_{gb})\right] . \tag{12}$$

Eqs. (11) and (12) establishe connection between the sampled current (i_{b0} and i_{c0}) and the average current.

3.2 Discontinuous operational mode

In this section the discontinuous current mode is presented. In the first step the continuous-discontinuous current threshold must be calculated.

At small load the current of the phase b becomes discontinuous. For calculating the continuous-discontinuous current threshold the maximal current of the phase b should be calculated.

The maximal current in phase b can be calculated from (8). Solved the equations:

$$i_{b\max} = i_{b0} + \frac{3U_{gb} + U_{dc}}{3L} t_{1f}. \tag{13}$$

If i_{bmax} is greater than zero (see Fig. 4) discontinuous current mode is occurred, because in continuous current mode the i_b current has to be always negative. In discontinuous current mode there are two different current modes depending on the load. These are *Disc1* and *Disc2* operational modes.

In the next subsections the two operational modes, the current waveforms of phase c and the main equations are presented.

3.2.1 Disc1 operational mode

In this state the current in phase b reaches zero before switching on 3L and $t_2 > t_1$.

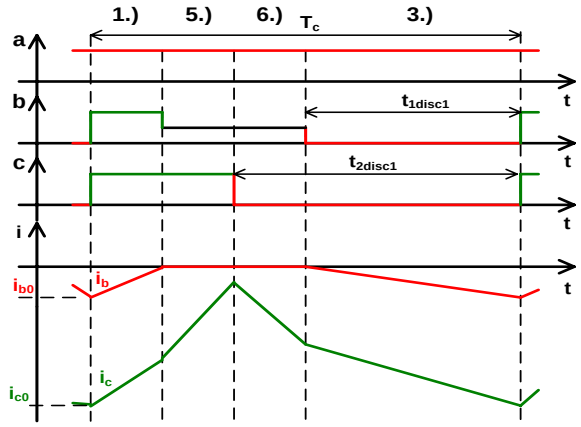

Fig. 5. Disc1 mode waveform

In Fig. 5 the current of the phases b and c, as well as the switching times can be seen. In phases a and c the current is always continuous, while in phase b during the section 5 and 6 the current is zero.

The change of rate of the inductor current in phase c during section 5 is:

$$\frac{di_{c5}}{dt} = \frac{u_{ga} - u_{gc}}{2L}, \tag{14}$$

while during section 6 is:

$$\frac{di_{c6}}{dt} = \frac{u_{ga} - u_{gc} - u_{dc}}{2L}. \tag{15}$$

3.2.2 Disc2 operational mode

In this state the current in phase b also reaches zero before switching on 3L but $t_1 > t_2$.

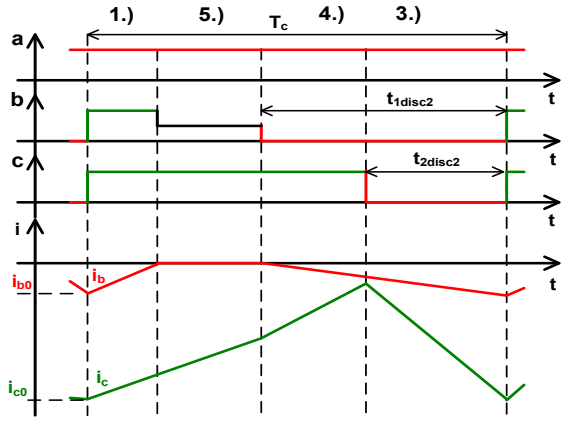

Fig. 6. Disc2 mode waveform

In Fig. 6 also the current of the phases b and c, as well as the switching times can be seen. In phases a and c the current is also always continuous, while in phase b during the section 5 it is zero.

The change of rate of the inductors current in phase b and c during the section 4 are:

$$\frac{di_{b4}}{dt} = -\frac{3u_{gb} + 2u_{dc}}{3L} \tag{16}$$

$$\frac{di_{c4}}{dt} = \frac{-3u_{gc} + u_{dc}}{3L}. \tag{17}$$

The operational mode depends on the current of the phase b and on the Disc1-2 threshold current.

The Disc1-2 threshold current can be calculated as follows:

$$i_{bdisc12} = T_c \frac{(3U_{gb} + U_{dc})(U_{gc} + 2U_{gb})}{3LU_{dc}} \quad . \tag{18}$$

Eq. (18) is true for instantaneous values, since the algorithm uses average values the average Disc1-2 threshold current has to be calculated.

Without demonstration the average value is the following:

$$i_{bdisc12AV} = \frac{t_{2disc12}^2}{2T_c}\frac{di_{b3}}{dt} - \frac{di_{b1}}{dt}\left(\frac{t_{2disc12}}{2T_c}\frac{di_{b3}}{di_{b1}}\right). \tag{19}$$

In steady state the start and end value of the current in the PWM cycle is equal. With this condition solved (18), the threshold current is:

$$\begin{aligned} i_{bdisc12} = &-\frac{T_c}{18U_{gb}U_{dc}^2L}\left[18U_{gb}^4 + 72U_{gc}(U_{gb}^3 + U_{gc}U_{gb}^2)\right. \\ &+9U_{dc}U_{gb}(U_{gb}^2 + 4U_{gc}U_{gb} + 4U_{gc}^2) \\ &\left.+U_{dc}^2(U_{gb}^2 + 4U_{gc}U_{gb} + 4U_{gc}^2)\right] \end{aligned} \quad . \tag{20}$$

If $i_{bavref} < i_{bdisc12}$, then *Disc1* operational mode occurs. Similarly to continuous mode in the first step the t_{1disc1} and t_{2disc1} switching times should be calculated.

Without demonstration the switching times can be calculated as follows:

$$t_{1disc1} = \sqrt{\frac{18T_cLi_{bdisc1ref}U_{gb}}{U_{dc}(3U_{gb} + U_{dc})}}, \tag{21}$$

$$t_{2disc1} = -T_c\frac{U_{gb} + 2U_{gc}}{U_{dc}}. \tag{22}$$

The current conduction time of the diode is:

$$t_{ddisc1} = \sqrt{\frac{2T_cLi_{bdisc1ref}(3U_{gb} + U_{dc})}{U_{gb}U_{dc}}}. \tag{23}$$

In the next step similarly to continuous mode the average value of phase c current is calculated. Without demonstration the average value is:

$$\begin{aligned} i_{cdisc1AV} = &-\frac{1}{4T_cL}\left[t_{2disc1}U_{dc} + T_c^2U_{gb} + 2T_c(T_cU_{gc}\right. \\ &-t_{ddisc1}U_{gb}) + t_{ddisc1}^2U_{gb} - t_{2disc1}^2U_{gb} \\ &-t_{1disc1}T_c(U_{gb} + 2U_{gc}) - t_{2disc1}(t_{2disc1}U_{gc} - t_{1disc1}U_{gb}) \\ &\left.+t_{2disc1}t_{1disc1}(U_{gc} + U_{ga} - U_{dc}) - t_{1disc1}t_{ddisc1}U_{gb}\right. \\ &\left.-t_{2disc1}^2U_{ga}\right] \end{aligned} \quad . \tag{24}$$

If $i_{bavref} > i_{bdisc12}$, then *Disc2* operational mode occurs. Similarly to *Disc1* mode in the first step the t_{1disc2} and t_{2disc2} switching times should be calculated. Without demonstrations the switching times can be calculated as follows:

$$\begin{aligned} t_{1disc2} = &\frac{T_c}{(9U_{gb}^2 - 4U_{dc}^2)U_{dc}} \\ &\left\{\left(U_{dc}\left(4U_{dc}U_{gc} + U_{gb}(2U_{dc} + 6U_{gc} + 3U_{gb})\right) + \sqrt{3P}\right)\right\} \end{aligned} \quad , \tag{25}$$

where

$$\begin{aligned} P = &T_c^2\left\{U_{gb}^2\{U_{dc}[9\ U_{gb}(8\ U_{gc}^2 + U_{gb}^2 + 4U_{gb}U_{gc})\right. \\ &-2U_{dc}\left(3U_{gb} + 4U_{dc}\right)\left(4U_{gc} + U_{gb}\right)] \\ &\left.-48U_{gc}^2U_{dc}\right\} - 32U_{dc}^3U_{gc}^2U_{gb}\Big\} \\ &+2T_ci_{bdisc2ref}LU_{dc}^2U_{gb}\left(U_{dc}\left(16U_{dc} + 9U_{gb}\right) - 27U_{gb}^2\right). \end{aligned}$$

Furthermore:

$$t_{2disc2} = -T_c\frac{U_{gb} + 2U_{gc}}{U_{dc}}, \tag{26}$$

$$t_{ddisc2} = -T_c\frac{6U_{dc}U_{gb}(12U_{gc} + U_{gb}) + \sqrt{3P}}{3U_{gb}U_{dc}(3U_{gb} - 2U_{dc})}. \tag{27}$$

Similarly to *Disc1* calculating the average value of the phase c current, without demonstration:

$$\begin{aligned} i_{cdisc2AV} = &\tfrac{-1}{12T_cL}\left\{3U_{gb}\left(t_{ddisc2}^2 + T_c^2\right)\right. \\ &+3T_c\left((2T_cU_{gc} - U_{gb}(2t_{ddisc2} + t_{2disc2})\right. \\ &-2t_{1disc2}^2\left(3U_{gb} + 2U_{dc}\right) + t_{2disc2}t_{1disc2} \\ &\left.\left.\left(4U_{dc} + 3U_{gb}\right) + 9t_{ddisc2}U_{gb} - 6T_cU_{gc}\right)\right\}. \end{aligned} \tag{28}$$

4 The control algorithm

In this section the control algorithm is given. The structure of the current controller for continuous current mode can be seen in Fig. 7.

The reference for the average phase currents (i_{bAVref} and i_{cAVref}) come from the DC voltage controller. According to (11) and (12) the difference between the sampled and average

values is estimated. Adding the average reference the result is the reference for the sampled value (i_{b0ref}, i_{c0ref}). Proportional control is used for the current control loop.

It is needed yet for the control the decoupling matrix **P** against the cross-coupling of the phases. The matrix contains two equations, which descript the contact between the change of the current of the other phase and the change of the voltage of the current phase. The results of the equations are as follows:

$$\Delta t_1 = -L\frac{di_c + 2di_b}{u_{dc}}, \tag{29}$$

$$\Delta t_2 = -L\frac{di_b + 2di_c}{u_{dc}}. \tag{30}$$

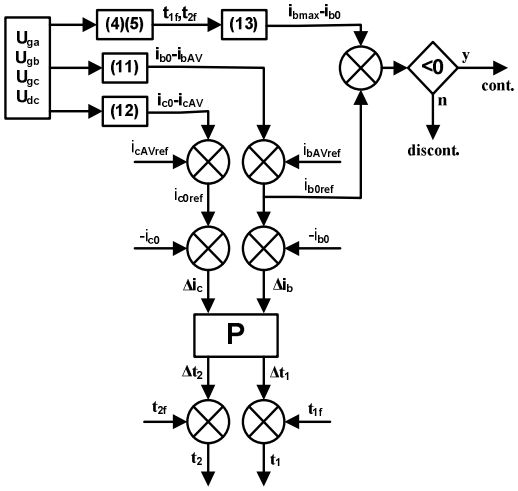

Fig. 7. Current controller for continuous current mode

The control structure is the same for discontinuous current mode, as well, but the equations should be substituted with the corresponding ones. In case of industrial PV converters not only differential mode but also common mode filters have to be used.

5 Experimental results

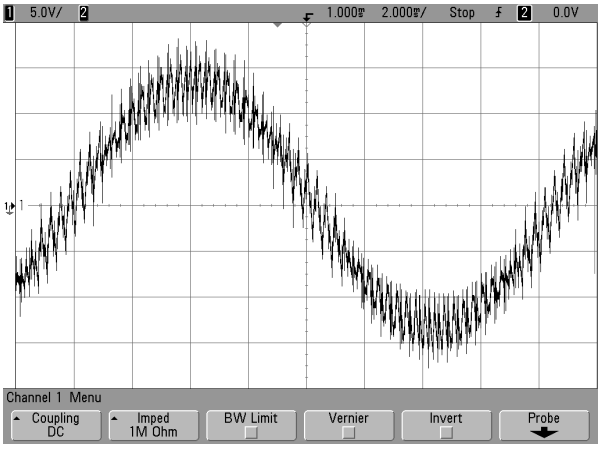

Fig. 8. Grid current waveform, space-vector control, 50% P_{nom}

The following measurements were taken on a PV converter of 250kW nominal power. The switching frequency was 2850Hz with synch modulation. The relative low switching frequency was necessary because of the prescribed high weighted efficiency (above 96%).

The first measurements were taken on about the half of the nominal power. The DC link voltage was 486V and 115kW power was injected into the grid. The grid current waveform in case of traditional d-q control and Space vector modulation can be seen on Fig. 8. In Figs. 8 and 9 the current resolution is 100Amp/division.

As it was discussed in Section 3 the current at zero-crossing in case of $d-q$ control changes with a small average value between positive and negative values causing significant switching and iron losses. Changing the control method to 3SC results the current waveform which can be seen in Fig. 9.

The last measurements were taken at 11% of the nominal power. The DC link voltage was 524V and 28kW power was injected into the grid. The grid current waveform in case of traditional d-q control and Space vector modulation can be seen on Fig. 10. In Fig. 10 and 11 the current resolution is 40Amp/division. With decreasing the load the switching frequency current component and the importance of 3SC control get much more important. In Fig. 11 it is seen that on small load the possible discontinuous current conduction area is wider and with 3SC more and more switching loss can be saved. Due the smaller current ripple the iron losses of the filter chokes will be smaller.

6 Conclusion

With the proposed 3SC and auxiliary CMCC control method on the presented topology a high performance, high efficiency converter was obtained even in the low radiation (less than 10% of nominal radiation) operating mode.

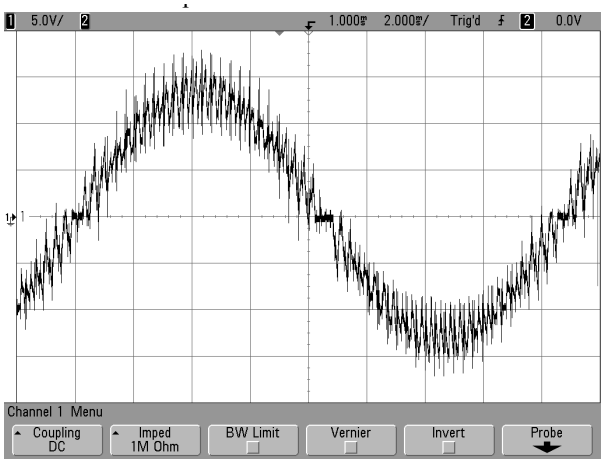

Fig. 9. Grid current waveform, 3SC control, 50% P_{nom}

With the using of this control the switching-on losses of the IGBT at current zero crossing was zero, the iron losses and the switching-off losses were much smaller than with the traditional

control. The 3SC was tested on 10kW and 250kW nominal power PV converters and has already been used in industrial PV converters many times in many countries.

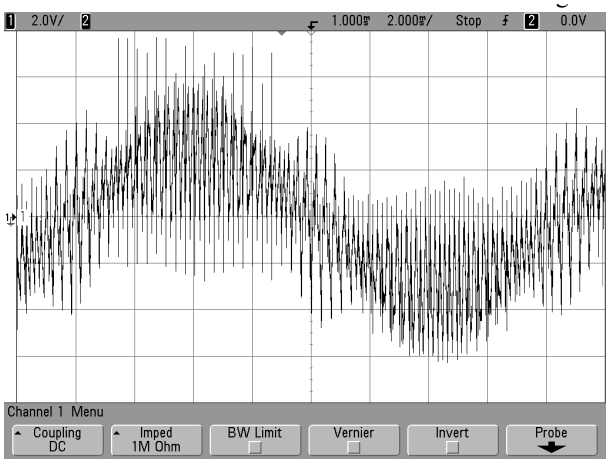

Fig. 10. Grid current waveform, space-vector control, 11% P_{nom}

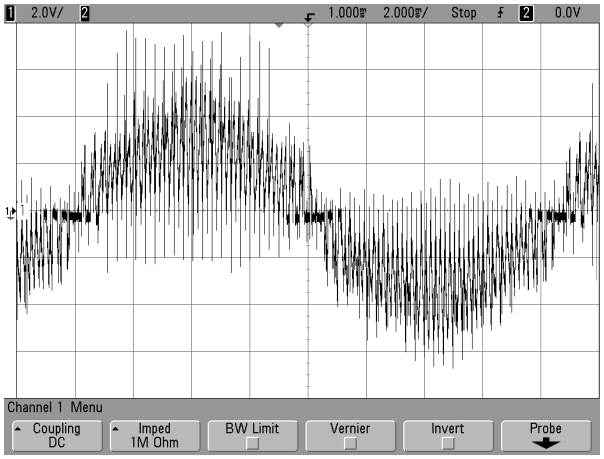

Fig. 11. Grid current waveform, 3SC, 11% P_{nom}

References

1 **Kyu Min Cho, Won Seok Oh, Young Tae Kim, Hee Jun Kim**, *A New Switching Strategy for Pulse Width Modulation (PWM) Power Converters*, Trans. on Industrial Electronics **54** (Feb. 2007), no. 1, 330-337.

2 **Li Peng, Yong Kang, Xuejun Pei, Jian Chen**, *A Novel PWM Technique in Digital Control*, Trans. on Industrial Electronics **54** (Feb. 2007), no. 1, 338-346.

3 **G. Escobar, A. A. Valdez, J. Leyva-Ramos, P. Mattavelli**, *Repetitive-Based Controller for a UPS Inverter to Compensate Unbalance and Harmonic Distortion*, Trans. on Industrial Electronics **54** (Feb. 2007), no. 1, 504-510.

4 **Ghias M A, Karimov K S, Termizi S I A, Mughal M J, Saqib M.A., Kazmi I H**, *A Photo-Voltaic System with Load Control Electrical Engineering*, 2007. ICEE '07. International Conference on 11-12 April 2007, pp. 1-5.

5 **Watanabe H., Shimizu T., Kimura G.**, *A novel utility interactive photovoltaic inverter with generation control circuit Industrial Electronics Society*, 1998. IECON '98. Proceedings of the 24th Annual Conference of the IEEE, April 31 Aug., pp. 721-725.

6 **Balogh A, Bilau Z T, Varjasi I**, *New Control Method for High Efficiency Grid Connected PV Converters*, Proc. of International Workshop – Control and Information Technology (IWCIT 2007), 2007.

7 _____, *High Efficiency Control of a Grid Connected PV Converter*, Proc. of Power and Energy Systems Conference (EuroPES 2007), 2007.

8 **Varjasi I**, *Discontinuous Current Mode of a Grid Connected PV Converter*, Proc. of International Youth Conference on Energetics (IYCE 2007), 2007.

9 **Varjasi I, Balogh A, Halász S**, *Sensorless Control of a Grid-Connected PV Converter 12th International Power Electronics and Motion Control Conference* (Aug. 2006), 901 – 906.